Molecular Cancer Therapeutics

Microvesicle-Mediated Delivery of Minicircle DNA Results in Effective Gene-Directed Enzyme Prodrug Cancer Therapy

Masamitsu Kanada[1,2,3,4], Bryan D. Kim[5], Jonathan W. Hardy[1,2,4,6], John A. Ronald[2,7,8,9], Michael H. Bachmann[1,2,4,6], Matthew P. Bernard[3,4], Gloria I. Perez[4], Ahmed A. Zarea[4], T. Jessie Ge[7], Alicia Withrow[10], Sherif A. Ibrahim[4,11], Victoria Toomajian[4,12], Sanjiv S. Gambhir[2,7,13,14], Ramasamy Paulmurugan[2,7], and Christopher H. Contag[1,2,4,6,12]

Abstract

An emerging approach for cancer treatment employs the use of extracellular vesicles, specifically exosomes and microvesicles, as delivery vehicles. We previously demonstrated that microvesicles can functionally deliver plasmid DNA to cells and showed that plasmid size and sequence, in part, determine the delivery efficiency. In this study, delivery vehicles comprised of microvesicles loaded with engineered minicircle (MC) DNA that encodes prodrug converting enzymes developed as a cancer therapy in mammary carcinoma models. We demonstrated that MCs can be loaded into shed microvesicles with greater efficiency than their parental plasmid counterparts and that microvesicle-mediated MC delivery led to significantly higher and more prolonged transgene expression in recipient cells than microvesicles loaded with the parental plasmid. Microvesicles loaded with MCs encoding a thymidine kinase (TK)/nitroreductase (NTR) fusion protein produced prolonged TK-NTR expression in mammary carcinoma cells. *In vivo* delivery of TK-NTR and administration of prodrugs led to the effective killing of both targeted cells and surrounding tumor cells via TK-NTR–mediated conversion of codelivered prodrugs into active cytotoxic agents. *In vivo* evaluation of the bystander effect in mouse models demonstrated that for effective therapy, at least 1% of tumor cells need to be delivered with TK-NTR–encoding MCs. These results suggest that MC delivery via microvesicles can mediate gene transfer to an extent that enables effective prodrug conversion and tumor cell death such that it comprises a promising approach to cancer therapy.

Introduction

A number of nucleic acid–based therapies for cancer are currently in various stages of preclinical and clinical evaluation (1, 2, 3). Among these, gene-directed enzyme prodrug therapy (GDEPT) delivers genes that encode and produce enzymes which selectively and locally convert systemically administered nontoxic or poorly toxic prodrugs into cytotoxic agents in the tumor. The converted agents then kill the cells expressing the prodrug-converting enzyme, as well as adjacent cells through the bystander effect. GDEPT has advantages over chemotherapy and radiotherapy, employing targeted release of therapeutics only at the disease site, and minimizing off-target side effects in normal tissues. This strategy has proven to be effective against many types of cancers (4). Viral vectors have been used for GDEPT, and because of their high transduction efficiency and absence of integration into the host genome, adenoviruses are the most commonly employed vector in clinical trials. However, the safety of using viral vectors remains a serious concern. Innate and acquired immune responses to the viral capsid proteins represent the most significant hurdle in the clinical application of adenoviral vectors for gene therapy (5). Nonviral gene delivery systems, such as synthetic lipid- or polymer-based nanocarriers, have been developed in attempts to circumvent these limitations. However, certain safety concerns including toxicities have impeded their clinical translation (6). The efficiency of gene delivery by the synthetic systems, and their rapid clearance from the circulation, predominantly by macrophages in the liver and spleen, has limited their utility (5, 7). With

[1]Department of Pediatrics, Stanford University, Stanford, California. [2]Department of Molecular Imaging Program at Stanford (MIPS), Stanford University, Stanford, California. [3]Department of Pharmacology & Toxicology, Michigan State University, East Lansing, Michigan. [4]Institute for Quantitative Health Science and Engineering (IQ), Michigan State University, East Lansing, Michigan. [5]Deptartment of Chemistry, University of California, Santa Cruz, California. [6]Department of Microbiology & Molecular Genetics, Michigan State University, East Lansing, Michigan. [7]Department of Radiology, Stanford University, Stanford, California. [8]Robarts Research Institute, Western University, London, Ontario, Canada. [9]Lawson Health Research Institute, London, Ontario, Canada. [10]Center for Advanced Microscopy, Michigan State University, East Lansing, Michigan. [11]Deptartment of Histology and Cell Biology, Faculty of Medicine, Mansoura University, Mansoura, Egypt. [12]Department of Biomedical Engineering, Michigan State University, East Lansing, Michigan. [13]Department of Bioengineering, Stanford University, Stanford, California. [14]Department of Materials Science, Stanford University, Stanford, California.

Note: Supplementary data for this article are available at Molecular Cancer Therapeutics Online (http://mct.aacrjournals.org/).

Corresponding Authors: Masamitsu Kanada, Michigan State University, 775 Woodlot Dr. East Lansing, MI 48824. Phone: (517) 884-6933; Fax: (517) 884-7463; E-mail: kanadama@msu.edu; Christopher H. Contag, Michigan State University, 775 Woodlot Dr. East Lansing, MI 48824. Phone: (517) 884-6933; E-mail: contagch@msu.edu; and Ramasamy Paulmurugan, Stanford University School of Medicine, 3155, Porter Drive, Room 2236, Palo Alto, CA 94304-5483. Phone: (650) 721-3306; E-mail: paulmur8@stanford.edu

Mol Cancer Ther 2019;18:2331–42

doi: 10.1158/1535-7163.MCT-19-0299

the current limitations of *in vivo* delivery systems, selective activation of prodrugs in cancer cells remains a promising, but as of yet unrealized, therapeutic approach (8).

Extracellular vesicles (EV) are natural delivery systems that mediate intercellular communications both locally and over distances during various physiologic and pathologic processes in the body (9, 10, 11). EVs have been proposed as vehicles for delivering therapeutic agents, due to their biocompatibility and potential to cross various biological barriers in the body relative to synthetic carriers (11). Compared with liposomes and lipid nanoparticles, exosomes, a major class of EVs, have been shown to successfully enter the dense stroma of pancreatic tumors and readily cross cellular membranes (12, 13). We have previously investigated whether exosomes and microvesicles, another major class of EVs, could deliver various biomolecules to recipient cells, and found that only microvesicles, not exosomes, can functionally deliver plasmid DNA into cells (14).

Several attempts have been made to increase therapeutic benefit of the GDEPT system and to minimize off-target effects by combining it with other therapeutic approaches. Coexpression of the herpes simplex virus thymidine kinase variant (HSV1-sr39TK) with caspase-3 has shown enhanced prodrug-mediated cell death in ovarian carcinoma cells (15, 16). Similarly, coexpression of nitroreductase (NTR) with murine granulocyte macrophage colony-stimulating factor was more effective in prodrug-mediated killing of TRAMP prostate cancer cell lines (17). Combining two suicide gene therapies significantly enhanced the therapeutic efficacy compared with each of the GDEPT systems used individually. The expression of a cycline deaminase/HSV1-sr39TK fusion gene significantly enhanced metabolic suicide and radio-sensitivity of glioma cells (18, 19). We recently created a HSV1-sr39TK-NTR fusion protein (TK-NTR) designed to catalyze two distinct cytotoxic mechanisms in cancer cells. First, HSV1-sr39TK results in the premature termination of DNA synthesis by activating nucleoside analog ganciclovir. Second, NTR prevents DNA replication by interstrand cross-linking through reducing the alkylating prodrug CB1954. We demonstrated the combined effects in several cancer types both *in vitro* and *in vivo* (20, 21, 22). The TK-NTR dual fusion gene achieved 5-fold higher cytotoxicity compared with its individual gene components delivered independently in metastatic triple-negative breast cancer, even though the delivery efficiency of the therapeutic gene(s) was relatively low (22).

To improve delivery of the two prodrug-converting enzymes for the GDEPT approach, we cloned the TK-NTR fusion gene into a minicircle (MC) DNA vector and examined delivery via microvesicles. MCs are circular DNA expression vectors that lack the prokaryotic backbone found in plasmids (23). Compared with their plasmid counterpart, MCs have improved transfection efficiencies and more prolonged transgene expression due to their smaller size and reduced transcriptional silencing (24). The mechanism of prolonged transgene expression is not well characterized but may result from eliminating heterochromatin formation induced by the plasmid backbone (25) and avoiding the acute inflammatory response to unmethylated CpG dinucleotide sequences found commonly in the backbone of plasmids (26, 27). Given the serious drawbacks associated with most viral vectors, MCs may constitute a safe vector for gene transfer (28), and with efficient delivery, may be used for effective cancer gene therapy in the clinic.

Materials and Methods

Plasmids and MC production

All plasmids were constructed using standard PCR cloning methods. The constructs were sequenced by either Sequetech (Mountain View) or the Stanford Protein and Nucleic Acid (PAN) Facility before using them for experiments. The *E. coli* strain ZYCY10P3S2T and the empty parental plasmid (PP) for MC production pMC.BESPX-MCS2 were purchased from System Biosciences (Palo Alto). The cytomegalovirus (CMV) promoter (CMVpro) and the improved firefly luciferase gene Luc2 (Promega) were PCR amplified and subcloned into the pMC.BESPX-MCS2 backbone containing an SV40 polyA and woodchuck hepatitis virus posttranscriptional element (WPRE) to generate PP-CMVpro-Luc2-WPRE (PP-fLuc). For the PP-TK-NTR construction, the CMVpro and the mutant HSV1-sr39TK-bacterial nitroreductase gene (NTR2) fusion was from our plasmid bank (Cellular Pathway Imaging Laboratory). The CMV-IEpro-TK-NTR construct was subcloned into the pMC-BESPX-MCS2 backbone. MC was produced following the protocol established previously (24). Briefly, ZYCY10P3S2T were transformed with the parental plasmid, followed by colony selection and overnight culture in Terrific Broth Medium (BioPioneer) containing kanamycin (50 μg/mL). To generate MCs, site-specific recombination via expression of C31 integrase and digestion of the bacterial backbone via expression of I-SceI endonuclease were initiated by the addition of equal volumes of LB containing 0.01% L-arabinose and 0.04 mol/L NaOH, after which cultures were grown for an additional 6 hours at 32°C. To generate parental plasmids, the bacteria were grown in the same medium without the addition of L-arabinose.

For stable expression, we constructed a *Sleeping Beauty* transposon, in which the TK-NTR fusion gene was under control of the CAG promoter, by subcloning it into the multiple cloning site of the pKT2/CAGXSP vector (M.H. Bachmann, manuscript in preparation) through recombination cloning (In-Fusion HD Cloning Kit, Clontech). TK-NTR was amplified by PCR using (forward) 5′-tggaattctgcagatagccgccaccATGGCTTCGTACCCCTGCCA and (reverse) 5′-gccactgtgctggatTTACACTTCGGTTAAGGTGATGTTTTGCG.

For the EV reporter, a palmitoylation sequence (MLCCMRRTKQ) of GAP43 was fused to EGFP (PalmGFP) by PCR as reported previously (29, 30), and PalmGFP was subcloned into the pKT2/CAGXSP.

Cell culture

The breast cancer cell lines 4T1 (from ATCC), MDA-MB-231, and MCF7 (a kind gift from Dr. Bonnie King, Department of Pediatrics, Stanford University, Stanford, CA), and BT474 (a kind gift from Dr. Mark Pegram, Department of Medicine, Stanford University, Stanford, CA) were cultured in DMEM supplemented with GlutaMAX (Gibco), 10% (vol/vol) FBS, and incubated at 37°C in a 5% CO_2 atmosphere.

EV isolation

EV-depleted FBS was prepared by 18-hour ultracentrifugation at 100,000 × *g*, 4°C (31). 4T1 cells were seeded at 7×10^5 cells or 1.5×10^6 cells per 60-mm or 100-mm cell culture dishes, respectively, and cultured in the EV-depleted medium, and microvesicles were then harvested as described previously (14). Briefly, conditioned medium was centrifuged at 600 × *g* for 30 minutes to remove cells and debris. The supernatant was centrifuged again at 2,000 × *g* for 30 minutes to remove apoptotic bodies.

Microvesicles were collected by ultracentrifugation at 20,000 × *g* for 60 minutes using Optima XL-90 Ultracentrifuge and 90Ti Rotor (Beckman Coulter), or refrigerated microcentrifuge 5424 R (Eppendorf) for small volumes. Supernatants were filtered through 0.22-μm membrane filters (Thermo Fisher Scientific) with pressure to remove large vesicles. Exosomes were collected by a size-based EV isolation method with modifications (32) using 50-nm membrane filters (EMD Millipore, VMWP02500) with holders (EMD Millipore, SX0002500). Briefly, holders with 50-nm membrane filters were connected to a vacuum manifold (Qiagen), and the membrane filters were first washed with 5–10 mL of PBS buffer by applying vacuum. Then, the remaining EVs including exosomes in the supernatant were trapped on the membranes. When approximately 100 μL of sample remained, the concentrated EVs were carefully collected.

Nanoparticle tracking analysis

Nanoparticle tracking analysis (NTA) was carried out using the Nanosight NS300 (Malvern Instruments) or the ZetaView (Particle Metrix) following the manufacturer's instructions. EVs derived from 4T1 cells with or without transfection were further diluted 100- to 1,000-fold with PBS for the measurement of particle size and concentration.

Western blotting

Equal numbers of EVs (6.8×10^8 EVs) derived from 4T1 cells were mixed with 4× sample buffer (Bio-Rad) with (for detecting ALIX, Rab27A, and Flotillin-1) or without (for detecting CD63) β-mercaptoethanol. Proteins were separated on a 4%–20% Mini-PROTEAN TGX gel (Bio-Rad) and transferred to a **polyvinylidene difluoride** membrane (Millipore, IPFL00010). After blocking with 5% ECL Blocking Agent (GE Healthcare, RPN2125) at room temperature for 1 hour, membranes were probed with primary antibodies overnight at 4°C at dilutions recommended by the suppliers as follows: anti-Alix (Proteintech, 12422), Rab27a (Proteintech, 17817), flottilin-1 (BD, 610820), CD63 (Thermo Fisher Scientific, 10628D, Ts63), followed by incubation with horseradish peroxidase (HRP)-conjugated secondary antibodies at room temperature for 1 hour. The membranes were visualized with ECL select Western Blotting Detection Reagent (GE Healthcare, RPN2235) on ChemiDoc MP Imaging System (Bio-Rad).

DNA loading in microvesicles

For efficient loading of plasmid DNA into microvesicles, 4T1 cells were seeded at 2×10^5 cells or 1.5×10^6 cells per 35-mm or 100-mm cell culture dishes, respectively, and transfected with parental plasmid or MC by lipofection (Lipofectamine 2000, Invitrogen, Thermo Fisher Scientific) following the protocol we previously established with slight modifications (14). Briefly, donor cells were incubated with lipofectamine/parental plasmid or MC complexes in DMEM without FBS for 8–12 hours. The transfected cells were gently rinsed with PBS and cultured in EV-depleted medium for 16–24 hours, followed by microvesicle isolation as described above.

Imaging flow cytometry was performed using an ImageStreamX MkII imaging cytometer, 60× magnification; with low flow rate/high sensitivity (EMD Millipore). To visualize microvesicles and loaded plasmid DNA, 4T1 cells were cotransfected with PalmGFP expression vector (30) and PP-fLuc that was prestained with Hoechst 33342 (H3570, Life Technologies) followed by microvesicle isolation. The data were analyzed using IDEAS Software (EMD Millipore).

For the analysis of DNA protection by microvesicle membranes, 4T1 cells were transfected with PP-fLuc or MC-fLuc to load them into microvesicles. The isolated microvesicles were then subjected to DNase I (62 Kunitz units/mL, RNase-free DNase Set, Qiagen) digestion (30 minutes at 37°C) to remove any DNA outside of the microvesicles. As a negative control, microvesicles were lysed before the DNase I treatment. The total DNA was isolated from the microvesicles (QIAamp DNA Mini Kit, Qiagen), and the *Luc2* gene was detected by PCR on C1000 Touch Thermal Cycler (Bio-Rad) using Platinum Hot Start PCR Master Mix (Invitrogen).

Real-time PCR was performed on a 7500 Fast Real-Time PCR System (Life Technologies, Thermo Fisher Scientific) in the Stanford PAN using SYBR Green PCR Master Mix (Life Technologies) with primers specific for Luc2, (forward) 5′-GGACTTGGACACCGGTAAGA and (reverse) 5′-GTCGAAGATGTTGGGGTGTT. Copy numbers of the *Luc2* gene were quantified using a standard curve method.

Fluorescence microscopy

Phase contrast and fluorescence images were taken using an EVOS FL Cell Imaging System (Life Technologies).

Transmission electron microscopy

Sample was prepared as previously reported with slight modifications (33). Isolated EVs were fixed in 2% paraformaldehyde for 5 minutes. For negative-staining of EVs, 5 μL of the sample solution was placed on a carbon-coated EM grid and EVs were immobilized for 1 minute. The grid was transferred to five 100 μL drops of distilled water and letting it for 2 minutes on each drop. The sample was negative stained with 1% uranyl acetate. The excess uranyl acetate was removed by contacting the grid edge with filter paper and the grid was air dried. The grids were imaged with a JEOL 100CXII transmission electron microscope operating at 100 kV. Images were captured on a Gatan Orius Digital Camera.

Flow cytometric analysis of CytoCy5S uptake in cells transfected with PP- or MC-TK-NTR and apoptosis assessment following treatment with prodrugs

4T1 cells in a 24-well plate were transfected with PP- or MC-encoded thymidine kinase-nitroreductase fusion protein (MC-TK-NTR). Cells were treated with CytoCy5S (100 ng/mL) for 3 hours. Median fluorescence intensity (MFI) of NTR/CytoCy5S was assessed. CytoCy5S$^+$ gating was based on untransfected controls without CytoCy5S treatment. For the apoptosis assay, 4T1 cells treated with prodrugs were stained with APC-conjugated Annexin V (BioLegend) according to the manufacturer's instructions. All flow cytometry data were acquired on a BD FACSAria IIu SORP instrument in the South Campus Flow Cytometry Core Facility at Michigan State University (East Lansing, MI) and analyzed with FCS Express software (v6; De Novo Software).

Generating 4T1 cells and MDA-MB-231 cells constitutively expressing firefly luciferase, EGFP, and TK-NTR

4T1 cells and MDA-MB-231 cells were cotransfected with a plasmid encoding firefly luciferase (fLuc) and EGFP-blasticidin resistance (BSD) fusion gene: pKT2/LuBIG (a kind gift from Drs. Andrew Wilber, Southern Illinois University, Springfield, IL; and

R. Scott McIvor, University of Minnesota, Minneapolis, MN; ref. 34) and pCMV(CAT)T7-SB100 (a kind gift from Dr. Zsuzsanna Izsvak, Max Delbrück Center for Molecular Medicine, Berlin, Germany, Addgene plasmid no. 34879; ref. 35). Transfected cells were selected in the presence of blasticidin (10 μg/mL) to establish cells constitutively expressing BSD-EGFP and fLuc (BGL). Selected cells were further cotransfected with pKT2/CAGXSP-TK-NTR and pCMV(CAT)T7-SB100. Transfected cells were selected in the presence of blasticidin (10 μg/mL) and puromycin (2 μg/mL) to establish cells constitutively coexpressing BGL and TK-NTR.

In vivo tumor studies

All procedures performed on animals were approved by Institutional Animal Care and Use Committees of Stanford University (Stanford, CA) or Michigan State University (East Lansing, MI). All mice were purchased from Charles River Laboratory. Female 8-week-old BALB/c nude mice were used for analysis of the bystander effect, and immunocompetent 8-week-old BALB/c mice were used for microvesicle-mediated GDEPT. The mice were either injected with 2.5×10^4 4T1-BGL cells with or without TK-NTR expression at subcutaneous sites to form tumors at six sites per mouse, or orthotopically injected with 2.5×10^4 4T1-BGL cells in mammary fat pads while under anesthesia (36). Ganciclovir (40 mg/kg) and CB1954 (40 mg/kg body weight) were mixed with 10% PEG400 (Sigma Aldrich) in PBS in 250 μL volume for each dose of prodrug combination and administered by intraperitoneal injection.

IHC

A portion of the tumor fixed in optimal cutting temperature (TissueTek) was sectioned at 7 μm in a Cryomicrotome and fixed in formal acetate for 10 minutes at room temperature, followed by an endogenous enzyme block with 0.3% hydrogen peroxide in Tris Buffered Saline (ScyTek Laboratories). All staining steps, apart from the primary antibody, were carried out on the intelliPATH automated IHC stainer at room temperature, utilizing auto-wash buffer between each staining reagent. Blocking for nonspecific binding utilized Mouse Block M (Biocare) for 10 minutes. The slides were incubated with polyclonal rabbit anti-active caspase-3 (ab2302; Abcam) overnight at 4°C in Normal Antibody Diluent (ScyTek Laboratories). Following the primary antibody, the reaction was completed by using ProMARK Rabbit on Rodent HRP polymer (Biocare) for 20 minutes and developed with Romulin AEC (Biocare). The slides were then counterstained with CATHE (1:10; Biocare) hematoxylin for 1 minute. Once the reaction was completed, the slides were rinsed with distilled water and allowed to air dry completely, followed by xylene and permanent mounting media.

Bioluminescence imaging

In vitro or *in vivo* assays for luciferase expression were performed with IVIS 50, IVIS 200, or IVIS Spectrum systems (Xenogen product line of Perkin-Elmer), which are located in the Stanford Center for Innovation in In-Vivo Imaging (http://med.stanford.edu/mips/aboutus/facilities/sci3.html) or the MSU IQ Imaging Core Facility. For *in vitro* assays, D-luciferin (300 μg/mL) was added to cultures prior to bioluminescence imaging (BLI). For *in vivo* imaging, mice were anesthetized with isoflurane using a SAS3 Anesthesia System (Summit Anesthesia Support) and an EVAC 4 waste gas evacuation system (Universal Vaporizer Support). After intraperitoneal injection of D-luciferin (150 mg/kg) emitted photons were captured as described previously (14), and bioluminescent signals were analyzed with Living Image Software (Perkin-Elmer).

Transwell assay

A HTS Transwell 96-Well Plate (Corning Inc., 3381 with 253380004) was used for this assay. The producer 4T1 cells coexpressing TK-NTR and fLuc, and the reporter 4T1 cells expressing fLuc were cultured in the top and bottom wells of the 96-transwell plate respectively, at 1×10^4 cells/well (Supplementary Fig. S6A). The cells were cultured for 4 days in the presence of prodrugs and used for BLI to assess the fLuc expression.

Statistical analyses

Student *t* test was performed for all statistical analyses and *P* values are indicated. Differences were considered to be statistically significant when the *P* value was less than 0.05.

Results

MCs encoding a fLuc enzyme achieved higher and prolonged transgene expression than plasmid DNA with parental backbone in breast cancer cells

We cloned the *fLuc* gene into parental plasmid DNA for expression from the CMV immediate early promoter resulting in PP-fLuc. From this, we created MCs (MC-fLuc) as described previously (24). PP-fLuc was approximately twice the size of MC-fLuc (Fig. 1A). Several murine and human breast cancer cell lines (4T1, MDA-MB-231, BT474, and MCF7) were transfected by lipofection (lipofectamine 3000) with either parental plasmid or MC encoding fLuc, using equimolar concentrations, and their fLuc expression levels were assessed and compared by imaging luciferase activity in cultures for up to 4 days (Fig. 1B). Irrelevant plasmid DNA was added to PP- or MC-fLuc to transfect cells with the same absolute amount of DNA. Transfection of either parental plasmid- or MC-expressing fLuc produced similar levels of bioluminescence at day 1. However, fLuc expression from MC-fLuc–transfected cells was sustained at higher levels over time relative to cells transfected with PP-fLuc. On day 4, the bioluminescent signal from cells transfected with MC-fLuc in the four cell types was on average 3.1 ± 0.5 (average $\pm$ SD) times greater than that generated by PP-fLuc (Fig. 1C). While the peak of fLuc expression level was not significantly different when equimolar amounts of PP-fLuc or MC-fLuc plasmids were transfected into breast cancer cells by lipofection (lipofectamine 3000), the duration of transgene expression from MC-fLuc–transfected cells was significantly longer than that from PP-fLuc–transfected cells.

Microvesicle-mediated delivery of MC-fLuc led to higher transgene expression than that of PP-fLuc in recipient cells

We previously reported that microvesicles can functionally transfer reporter molecules from donor to recipient cells, and specifically deliver plasmid DNA (14). Following the protocol that we previously described for loading plasmids into microvesicles, 4T1 cells were transiently transfected with equimolar amounts (same copy numbers) of PP-fLuc or MC-fLuc. The isolation of microvesicles was performed by differential ultracentrifugation. Sizes and numbers of the isolated microvesicles containing PP-fLuc or MC-fLuc were analyzed by NTA. The mean

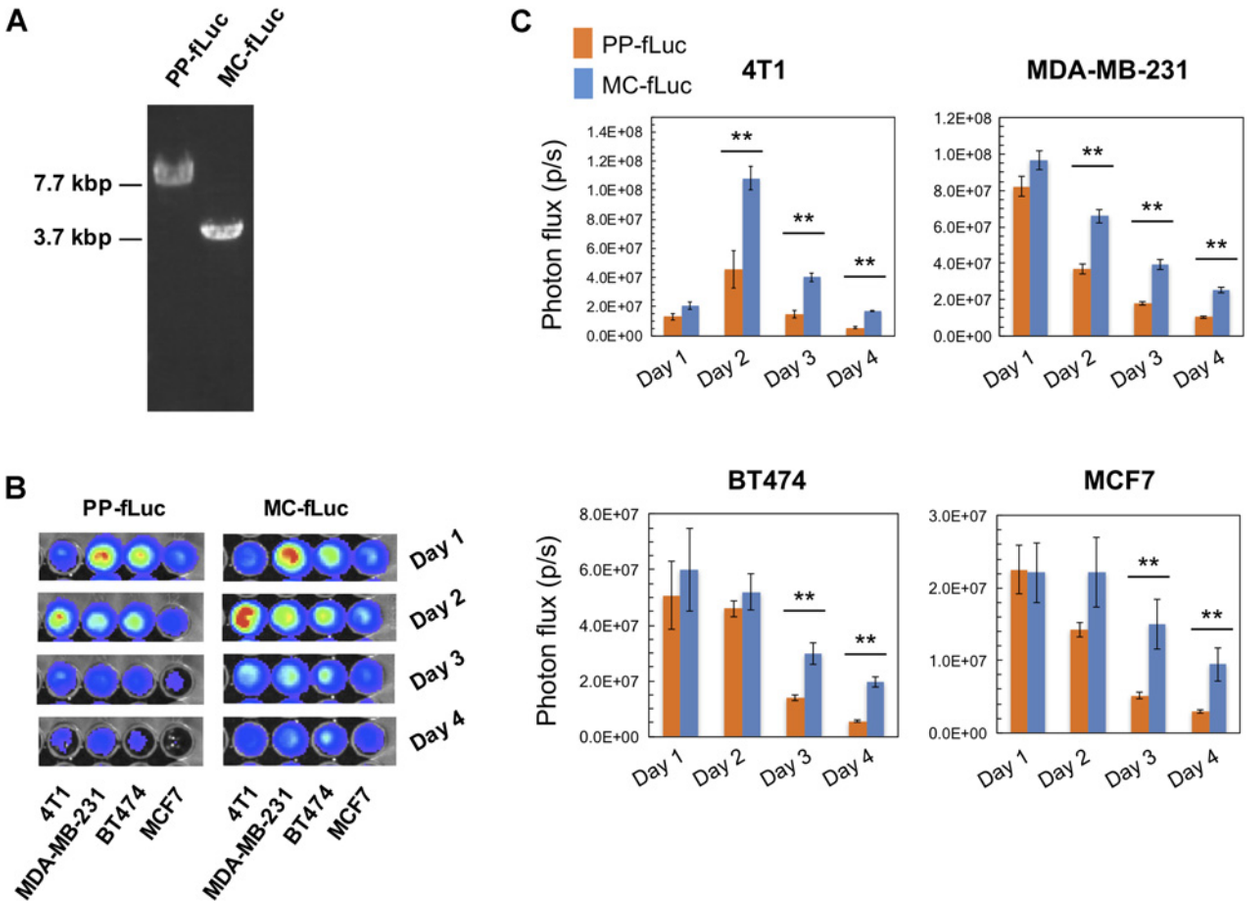

Figure 1.

Comparison of the transgene expression of MC-fLuc and PP-fLuc in breast cancer cells. **A,** Agarose gel electrophoresis confirming the ability to generate both PP- and MC-fLuc. DNAs were digested with *Bam*HI. **B,** Bioluminescence in murine (4T1) and human (MDA-MB-231, BT474, and MCF7) breast cancer cells transfected with equimolar PP- or MC-fLuc. **C,** Time course measurement of bioluminescence in the breast cancer cells transfected with PP- (orange) or MC-fLuc (blue) represented in (**B**). Error bars, SD ($n = 3$; **, $P < 0.01$).

sizes of microvesicles without modification, loaded with PP-fLuc, or MC-fLuc were all similar (136, 160, and 145 nm, respectively; Fig. 2A). Microvesicles are generally regarded as larger vesicles (50–1,000 nm in diameter), but the majority of the isolated microvesicles derived from 4T1 cells exhibited the size range of exosomes (40–120 nm in diameter). We then isolated exosome- and microvesicle-enriched fractions. The morphology and sizes of these two EV fractions were characterized by transmission electron microscopy (TEM), and the expression of exosome marker proteins such as ALIX, CD63, Flottilin-1, and Rab27a by Western blot analysis. Consistent to NTA, the diameters of the majority of microvesicles were smaller than 200 nm and an artefactual cup-shaped morphology was observed by TEM (ref. 9; Supplementary Fig. S1A). The mean sizes of the isolated exosomes and microvesicles were 115 and 140 nm in diameter, respectively (Supplementary Fig. S1B). In addition, the exosome fractions dominantly expressed Alix, CD63, and Rab27a, while only slight expression of these markers was detected in the microvesicle fraction (Supplementary Fig. S1C). The expression level of Flotillin-1 was higher in the fraction of microvesicles than that of exosomes. These results indicate that EVs isolated from 4T1 cells by 20,000 × *g* ultracentrifugation mainly includes microvesicles, and the remaining EVs contains predominantly exosomes.

We next assessed the association of PP-fLuc and microvesicles by imaging flow cytometry. PP-fLuc was prestained with Hoechst 33342, and 4T1 cells were cotransfected with both the stained PP-fLuc and the plasmid vector encoding the membrane-binding GFP (PalmGFP; ref. 30), followed by the isolation of the microvesicles (Supplementary Fig. S2A). Flow cytometric analysis showed that 1% of the total microvesicles were PalmGFP positive and associated with the prestained PP-fLuc (Supplementary Fig. S2B and S2C). Because double-stranded genomic DNA was associated with the outside of EVs (37), we tested protection of the loaded DNA by the microvesicle membranes. The loaded PP-fLuc or MC-fLuc were protected from degradation by a DNase I treatment, indicating that the loaded DNA was confined inside the microvesicles (Supplementary Fig. S2D). We further analyzed total copy numbers of PP-fLuc or MC-fLuc encapsulated in the microvesicles by q-PCR, and the copy numbers were further divided by the microvesicle numbers to determine the DNA copy number per microvesicle. On average, there were 0.13 ± 0.02

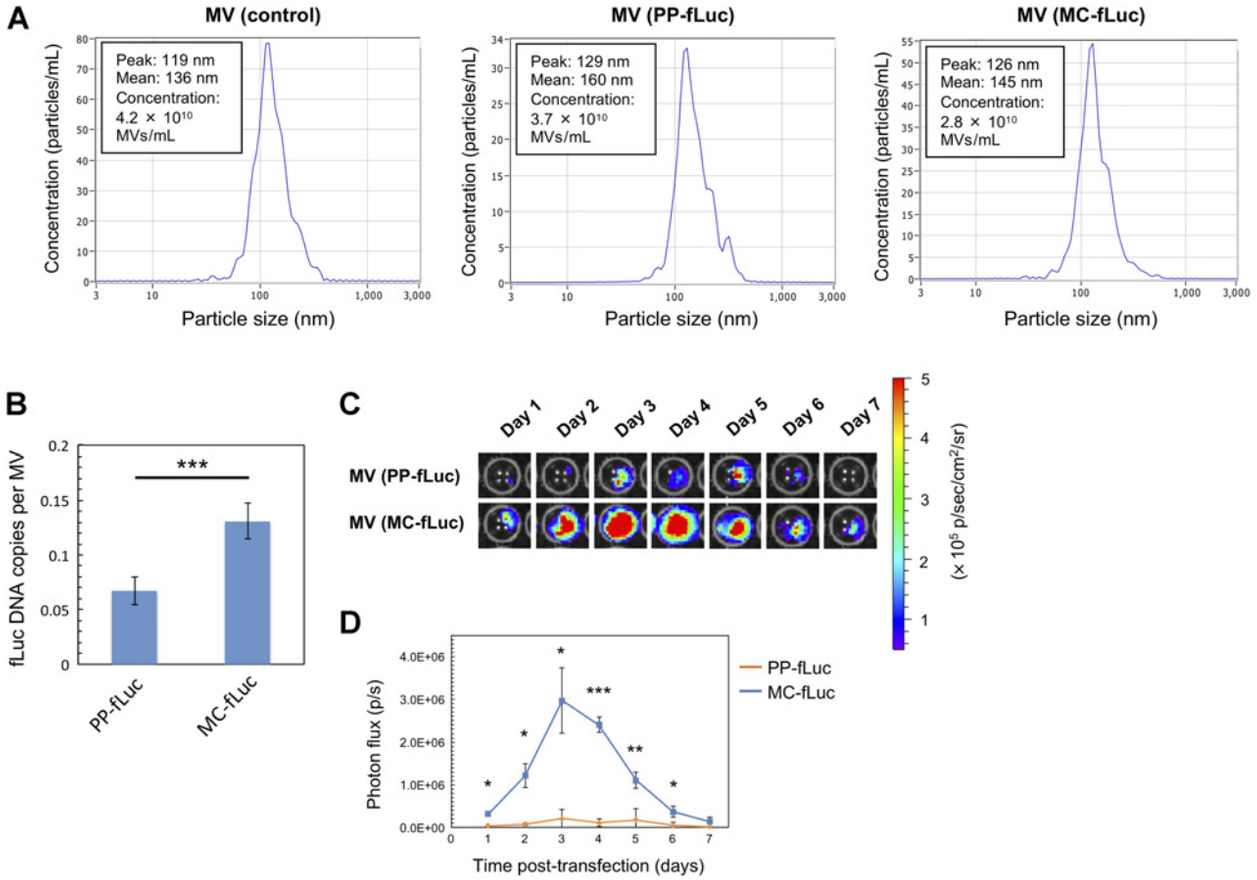

Figure 2.

Microvesicle-mediated delivery of PP- or MC-fLuc. **A,** NTA of unmodified or modified microvesicles derived from 4T1 cells. **B,** Analysis of fLuc DNA copy numbers in individual microvesicles. Error bars, SD ($n = 3$), ***, $P < 0.001$. **C,** Microvesicle-mediated fLuc transfer in 4T1 cells. Recipient 4T1 cells were cultured with microvesicles derived from 4T1 cells transiently transfected with equimolar PP- or MC-fLuc. **D,** Time course measurement of bioluminescence in the recipient cells that took up microvesicles containing PP- (orange) or MC-fLuc (blue). Photon flux (photons/second) is plotted over time (days). Error bars, SD ($n = 3$; *, $P < 0.05$; **, $P < 0.01$; ***, $P < 0.001$).

(average ± SD) copies of MC-fLuc per microvesicle, compared with 0.067 ± 0.01 copies of PP-fLuc per microvesicle (average ± SD; Fig. 2B). Thus, MC-fLuc was encapsulated into microvesicles at approximately twice the efficiency as PP-fLuc, and incidentally, PP-fLuc is approximately twice the size of MC-fLuc. Next, we assessed microvesicle-mediated delivery of PP-fLuc and MC-fLuc using luciferase activity in recipient cells as a readout. Microvesicles were isolated from 4T1 cells transfected with equimolar concentrations of either PP-fLuc or MC-fLuc. Microvesicles containing PP-fLuc (2.5×10^9 microvesicles/well) or microvesicles containing MC-fLuc (1.9×10^9 microvesicles/well) were added to untreated 4T1 cells in a 96-well plate and incubated overnight. Both constructs resulted in the bioluminescence signals that increased over a 3-day period (Fig. 2C). Microvesicles containing MC-fLuc led to a peak bioluminescence signal in the recipient cells that was approximately 14-times higher than that induced in cells treated with microvesicles containing plasmid DNA, PP-fLuc (Fig. 2D). While the loading efficiency of MC-fLuc was only twice that of PP-fLuc, the resulting expression of fLuc in the recipient cells were 14-times greater, indicating that there are benefits in both loading and transfer.

MC-TK-NTR showed greater activity of prodrug-converting enzymes than PP-TK-NTR

We next tested the potential application of microvesicle-mediated MC delivery of GDEPT. The two well-studied enzyme/prodrug combinations, which include TK/ganciclovir and NTR/CB1954 (4), were used. TK and NTR convert their respective nontoxic prodrugs into active cytotoxic agents, which then specifically kill the cells expressing the enzymes, as well as neighboring tumor cells and stromal cells in the tumor microenvironment through the bystander effect. To combine this GDEPT with microvesicle-mediated MC delivery, we cloned the TK-NTR fusion gene under control of the CMV-IE promoter into a parental plasmid (PP-TK-NTR) and produced a MC derivative (MC-TK-NTR; Fig. 3A). To test the activity of the encoded NTR we used CytoCy5S, a Cy5-labeled quenched substrate of NTR that acts as an imaging agent to measure NTR enzyme activity (38). To compare the maximum gene expression from the two TK-NTR delivery vectors, 4T1 cells were transfected with an equal mass

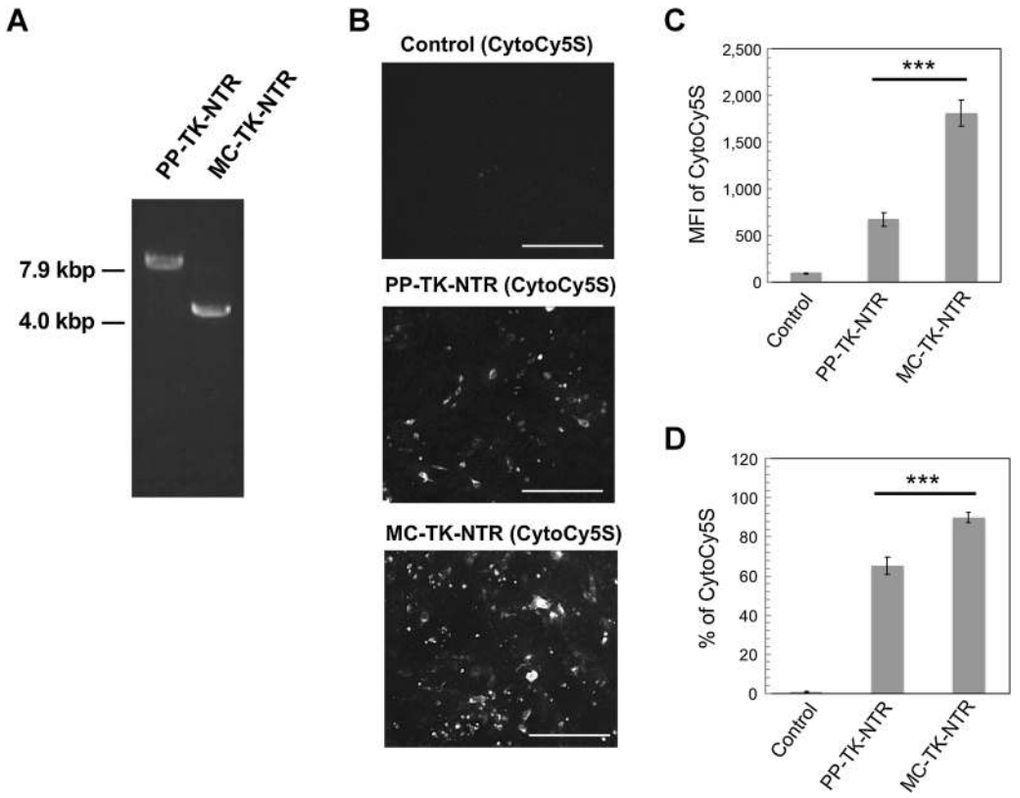

Figure 3.

NTR activity measured in 4T1 cells transfected with PP- or MC-TK-NTR by CytoCy5S assay. **A,** Agarose gel electrophoresis of PP- (~7.9 kbp) and MC-TK-NTR (~3.9 kbp). **B,** Fluorescence images of 4T1 cells transfected with PP- or MC-TK-NTR 3 hours after exposure to CytoCy5S, a quenched fluorescent substrate of NTR. Scale bars, 400 μm. **C,** Analysis of the MFI of CytoCy5S in 4T1 cells without transfection (control), with PP-TK-NTR, or with MC-TK-NTR. Error bars, SD ($n = 3$), ***, $P < 0.001$. **D,** Analysis of the percentage of NTR/CytoCy5S cells as in **C**. Error bars, SD ($n = 3$; ***, $P < 0.001$).

(200 ng/well in a 96-well plate and 800 ng/well in a 24-well plate) of PP- or MC-TK-NTR by lipofection. Cells were incubated with CytoCy5s, and NTR expression was assessed by fluorescence microscopy and flow cytometry. A larger number of 4T1 cells transfected with MC-TK-NTR showed NTR activity compared with the cells transfected with PP-TK-NTR (Fig. 3B). Cellular CytoCy5s fluorescence was quantified in 4T1 cells by flow cytometry. 4T1 cells transfected with MC-TK-NTR showed 2.7-times higher CytoCy5S MFI and 1.4-times more cells were positive for CytoCy5S fluorescence compared with the cells transfected with PP-TK-NTR (Fig. 3C and D, respectively; Supplementary Fig. S3). These results indicate that MC-TK-NTR is a more effective gene expression vector under these conditions compared with PP-TK-NTR, and therefore likely more suitable for GDEPT.

MC-TK-NTR more effectively induced apoptosis than PP-TK-NTR in cancer cells in response to prodrugs

We determined the minimum gene expression from PP- or MC-TK-NTR necessary to kill cancer cells when they are treated with the prodrug combination. Reporter 4T1 cells constitutively expressing fLuc in a 96-well plate (1.2×10^4 cells/well) were transfected with a 10-fold dilution series of equal masses of PP- or MC-TK-NTR (0, 0.2, 2, 20, and 200 ng). Unrelated plasmid DNA was added to PP- or MC-TK-NTR DNA to transfect cells with the same total mass of DNA. After treatment with the prodrugs, ganciclovir (3.9 μmol/L) and CB1954 (10 μmol/L), the cells' bioluminescence levels were measured as an indicator of cellular viability (Fig. 4A). Reporter 4T1 cells that were transfected with 20 ng of the plasmid, PP-TK-NTR, showed a cell death rate of 70% in response to prodrug combination treatment, as indicated by a reduction in bioluminescent signal, while transfection of smaller amounts of this plasmid yielded no significant cell killing (Fig. 4B). In contrast, transfection of 0.2 ng of MC DNA, MC-TK-NTR, into the reporter 4T1 cells, resulted in a reduction of 46% in bioluminescent signal (Fig. 4A and B). This result indicated that approximately 100-times less MC DNA (MC-TK-NTR) than plasmid DNA (PP-TK-NTR) is needed to significantly kill 4T1 cells in culture. Induction of apoptosis in cells that expressed the TK-NTR fusion proteins and cotreated with the prodrugs was confirmed with a flow cytometric analysis. The outer cell-surface membrane indicator of apoptosis, phosphatidylserine, was detected using APC-conjugated Annexin V (Fig. 4C; refs. 39, 40). For flow cytometric analysis, reporter 4T1 cells in a 24-well plate (5×10^4 cells/well) were transfected with a 10-fold dilution series of equal masses of PP- or MC-TK-NTR (0, 0.8, 8, 80, and 800 ng), followed by the treatment with the prodrugs, ganciclovir and CB1954. The expression of MC-TK-NTR fusion

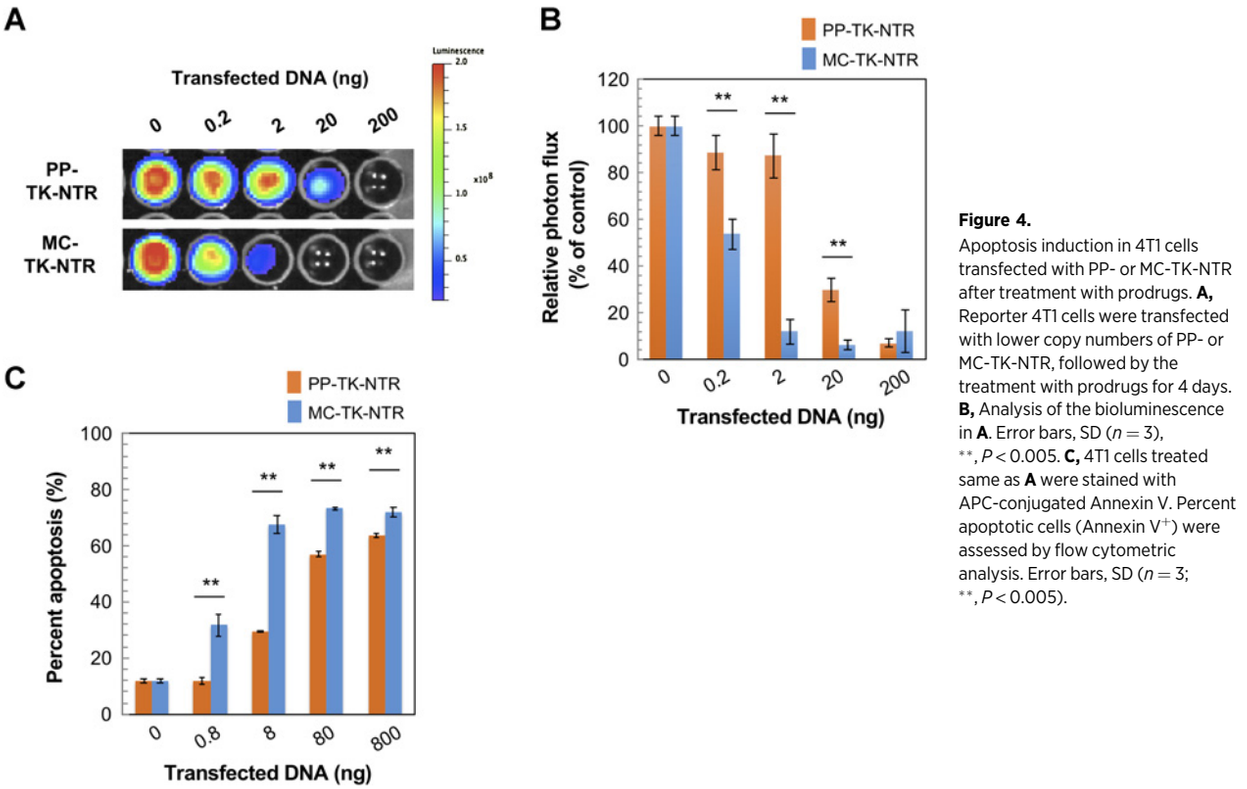

Figure 4.
Apoptosis induction in 4T1 cells transfected with PP- or MC-TK-NTR after treatment with prodrugs. **A,** Reporter 4T1 cells were transfected with lower copy numbers of PP- or MC-TK-NTR, followed by the treatment with prodrugs for 4 days. **B,** Analysis of the bioluminescence in **A**. Error bars, SD ($n = 3$), **, $P < 0.005$. **C,** 4T1 cells treated same as **A** were stained with APC-conjugated Annexin V. Percent apoptotic cells (Annexin V^+) were assessed by flow cytometric analysis. Error bars, SD ($n = 3$; **, $P < 0.005$).

proteins significantly increased the percent of Annexin V-positive 4T1 cells compared with PP-TK-NTR at all plasmid concentrations in the presence of prodrugs (Fig. 4C).

TK-NTR–expressing cells activated cytotoxic prodrugs that diffused into neighboring cancer cells and induced their death via bystander effect

Key features of GDEPT are cell-specific gene delivery and expression, controlled conversion of prodrugs to cytotoxic agents, and expansion of cell killing to the neighboring cells via diffusion of the active agents in a bystander effect (4). To determine the effectiveness of prodrug conversion by TK-NTR and subsequent bystander killing, we generated 4T1 cells and human breast cancer MDA-MB-231 cells constitutively expressing the TK-NTR gene fusion, fLuc, and EGFP using *Sleeping Beauty* transposons (41). Constitutive expression of TK-NTR in both cell types was confirmed by exposing the transfected cells to CytoCy5s. Most of the 4T1 and MDA-MB-231 cells expressing TK-NTR, fLuc, and EGFP activated CytoCy5S, while no activation of CytoCy5S was detected from control 4T1 or MDA-MB-231 cells constitutively expressing only fLuc and EGFP (Supplementary Fig. S4).

The fLuc-EGFP reporter 4T1 or MDA-MB-231 cells were cocultured with different percentages of the TK-NTR producer 4T1 or MDA-MB-231 cells, respectively, in the presence of ganciclovir (3.9 μmol/L) and CB1954 (10 μmol/L). The reporter cells cocultured with 25% and 50% of the producer cells reduced the bioluminescence signal by more than 50% in both 4T1 and MDA-MB-231 cells (Fig. 5A and B; Supplementary Fig. S5A and S5B). These results suggested that activated cytotoxic agents from the producer cells readily diffuse into the neighboring cancer cells. Furthermore, induction of apoptosis in bystander cells cocultured with the TK-NTR producer 4T1 cells was confirmed with flow cytometric analysis of outer cell-surface membrane phosphatidylserine using APC-conjugated Annexin V. Reporter 4T1 cells in a 24-well plate were cocultured with different percentages of the producer cells. Increased percentages of the producer cells significantly increased the numbers of Annexin V-positive 4T1 cells in the presence of prodrugs (Fig. 5C). The mechanism of the bystander effect in the prodrug combination treatment may include a number of factors. Because the HSV-TK/ganciclovir system apparently requires cell–cell contact to display a bystander effect (42), we further assessed the contribution of direct cell contact between the TK-NTR producer cells and the reporter cells to the bystander effect by using a transwell assay. The reporter 4T1 cells were cocultured with the same number of producer cells using 0.4-μm transwell membranes (Supplementary Fig. S6A). The cells' bioluminescence levels were measured as an indicator of cell viability. The bioluminescence signals in the reporter cells on the bottom wells were increased by 1.7-fold, while the signals in the producer cells on the top wells were severely reduced when treated with prodrug combination (Supplementary Fig. S6B and S6C). This result indicates that the toxic metabolites created in the producer cells do not spread efficiently to neighboring cancer cells without cell–cell contact.

We next asked how many cancer cells need to express TK-NTR to confer the therapeutic effects of the prodrug treatment *in vivo*. Six tumors were created by subcutaneously implanting 2.5×10^4 reporter 4T1 cells containing different percentages of the producer 4T1 cells (0%, 0.5%, 1%, 5%, 25%, and 50% within the population of total 4T1 cells) into athymic nude mice. Each nude mouse harboring six tumors received two doses of the prodrug combination (ganciclovir, 40 mg/kg and CB1954, 40 mg/kg) day

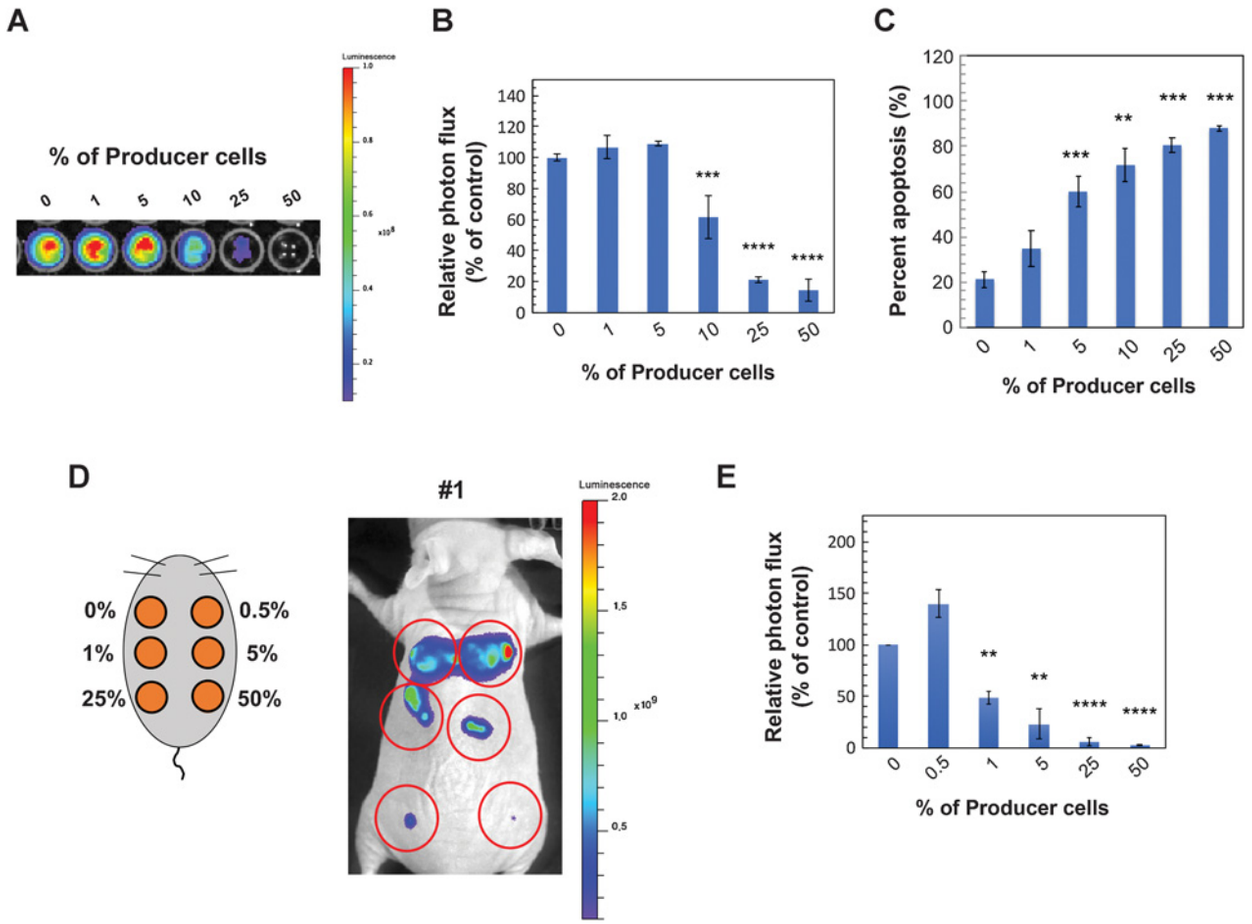

Figure 5.

Efficient diffusion of activated cytotoxic agents from producer cells into cocultured cells and in mice. **A,** Reporter 4T1 cells cocultured with different percentages of 4T1 cells stably expressing TK-NTR after the treatment with prodrugs for 4 days. **B,** Analysis of the bioluminescence in **A**. Error bars, SD ($n = 3$), ***, $P < 0.001$; ****, $P < 0.0001$. **C,** 4T1 cells treated same as **A** were stained with APC-conjugated Annexin V. Percent apoptotic cells (Annexin V^+) were assessed by flow cytometric analysis. Error bars, SD ($n = 3$), **, $P < 0.01$; ***, $P < 0.001$. **D,** Positions of subcutaneous tumors containing different percentages of TK-NTR expressing 4T1 cells (0%, 0.5%, 1%, 5%, 25%, and 50% within a population of wild-type 4T1 cells (left). Cell killing effects of tumors containing different percentages of TK-NTR-expressing 4T1 cells in nude mice after the treatment with prodrugs (right). **E,** Analysis of the bioluminescence from the tumors (red circles indicated in **D**). Error bars, SEM ($n = 3$), **, $P < 0.01$; ****, $P < 0.0001$ compared with the value of control.

2 and 6 after cancer cell implantation. *In vivo* BLI was performed at day 9 to assess tumor growth in the mice (Fig. 5D; Supplementary Fig. S7). There was apparent cancer cell killing in the tumors containing 1%, 5%, 25%, and 50% of the producer cells, while tumors containing 0% and 0.5% of the producer 4T1 cells were unaffected (Fig. 5E). Under the constraints of our experimental approach, this result suggests that *in vivo* delivery of the TK-NTR fusion gene to at least 1% of the total tumor cells followed by prodrug combination treatment has significant therapeutic potential. We therefore aimed to achieve the best possible delivery of the TK-NTR fusion gene by using MC for gene expression and packaging it into microvesicles for effective *in vivo* delivery.

Intratumoral injection of microvesicles containing MC-TK-NTR and prodrug combination treatment eliminated breast cancer cells *in vivo*

To demonstrate the efficacy of microvesicle-mediated delivery of MC-TK-NTR as a potential GDEPT, we first assessed *in vitro* cell killing effect after treatment with the prodrug combination. Microvesicles (4.5×10^{10}) were isolated from 4T1 cells transfected with an equal mass of PP- or MC-TK-NTR in a 100-mm cell culture dish. One-third of the isolated microvesicles (1.5×10^{10}) were added to reporter 4T1 cells in a 96-well plate and incubated overnight, followed by treatment with prodrugs for 4 days. Microvesicles containing PP- and MC-TK-NTR resulted in 60% and 73% cell killing, respectively, relative to reporter 4T1 cells treated with unmodified microvesicles derived from 4T1 cells (Fig. 6A and B).

To determine the therapeutic efficacy of microvesicle-mediated delivery of MC-TK-NTR *in vivo*, we employed mouse breast cancer models by orthotopically implanting 2.5×10^4 reporter 4T1 cells constitutively expressing fLuc to form two tumors in mammary fat pads of immunocompetent BALB/c mice. All tumors became palpable 16 days after the initial implantation. The animals ($n = 24$) were split into six groups (4 animals with two tumors each in a group) for each treatment ($n = 8$ for each group). TK-NTR–loaded or unmodified microvesicles (4.5×10^{10}) were

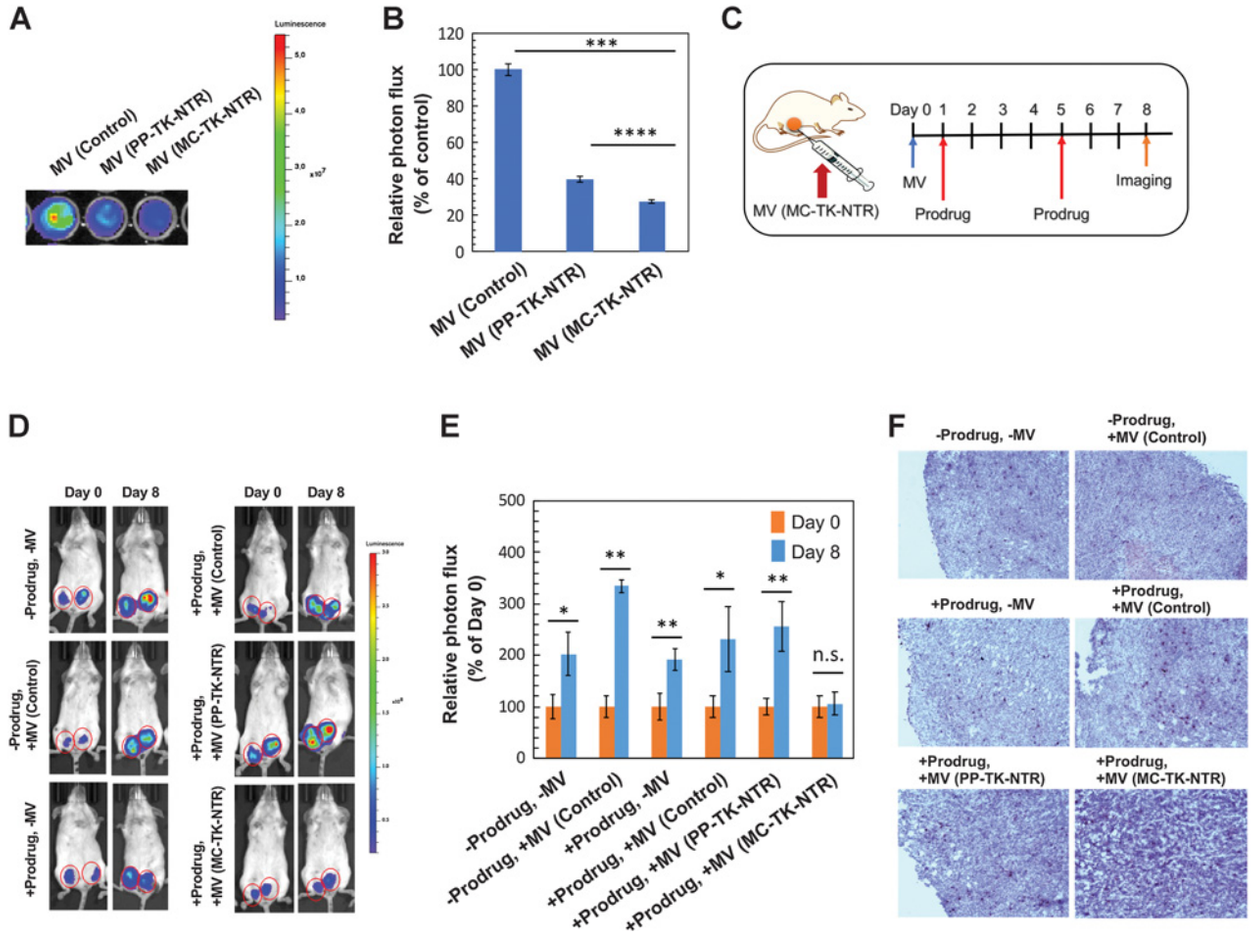

Figure 6.

Microvesicle-mediated intratumoral delivery of MC-TK-NTR for prodrug therapy. **A,** 4T1 cells expressing fLuc were cultured with the isolated MVs derived from 4T1 cells transiently transfected with PP- or MC-TK-NTR, followed by prodrug treatment for 4 days. **B,** Analysis of the bioluminescence in **A**. Error bars, SD ($n = 3$), ***, $P < 0.001$; ****, $P < 0.0001$. **C,** Schematic illustration for the MV-mediated MC-TK-NTR delivery and prodrug treatments. **D,** Bioluminescence images of representative animals bearing two tumors for each treatment group. **E,** Analysis of the bioluminescence from tumors treated with prodrugs and MVs containing PP- or MC-TK-NTR. Error bars, SEM ($n = 5, 4, 8, 6, 8, 8$, respectively). *, $P < 0.05$; **, $P < 0.01$; n.s., not significant. **F,** Active caspase-3 staining of tumor tissues of animals treated with different MVs.

injected directly into one site in the tumors at day 0. A combination of ganciclovir (40 mg/kg) and CB1954 (40 mg/kg) was injected intraperitoneally into the mice at day 1 and day 5 (Fig. 6C). The tumor development and growth were monitored at day 0 and day 8 by measuring bioluminescence signals in the tumors (Fig. 6C). Intratumoral delivery of MC-TK-NTR via microvesicles followed by prodrug combination treatment significantly reduced the bioluminescent signal by 54% relative to the tumors treated with unmodified microvesicles over 8 days (Fig. 6D and E). However, the tumors injected with microvesicles carrying PP-TK-NTR showed no significant suppression of tumor growth compared with the tumors injected with unmodified microvesicles (Fig. 6E). This may be due to the insufficient expression of TK-NTR produced from the plasmids in the tumors. The tumors were excised for histologic analysis. Active caspase-3 staining of the tumors injected with microvesicles carrying MC-TK-NTR showed higher levels of apoptotic cells compared with the tumors in other groups (Fig. 6F).

Discussion

We have developed a novel GDEPT approach comprised of a MC-TK-NTR, which is efficiently delivered by microvesicles to cancer cells and induces both direct and bystander killing of tumor cells after administration of the two respective prodrugs. Our prior study had shown that plasmid DNA encoding reporter genes that were endogenously encapsulated into microvesicles can be functionally delivered to recipient cells (14). However, the efficiency of the microvesicle-mediated delivery of plasmid DNA needed to be improved for the development of a therapeutic gene delivery system. Compared with delivery of the parental plasmid, PP-TK-NTR, we found that a significantly lower amount of microvesicles carrying MC-TK-NTR was sufficient for achieving a therapeutic effect after a prodrug combination treatment in recipient cancer cells. This difference was due to both higher expression of TK-NTR enzymes from MCs, and prolonged expression of the enzymes which complemented their slow induction of apoptosis during prodrug treatment (22). Analysis of endogenous loading

of MC-fLuc into microvesicles showed that MCs were more efficiently loaded into microvesicles than plasmid DNA. More importantly, MC-fLuc expressed far more fLuc in target cancer cells than PP-fLuc, because their smaller size resulted in more efficient loading into microvesicles and elimination of the plasmid backbone prolonged transgene expression (Fig. 2). Finally, we demonstrated that cytotoxic agents created from the prodrugs in cancer cells expressing TK-NTR readily diffused into neighboring cells mainly through cell-to-cell contact and effectively triggered cell death in nontransfected cells both *in vitro* and *in vivo* (Fig. 5; Supplementary Fig. S6).

EV-mediated GDEPT has previously been proposed (43, 44, 45). EV-mediated delivery of mRNA/protein of cytosine deaminase fused to uracil phosphoribosyltransferase (CD-UPRT) were delivered to the schwannoma tumors in an orthotopic mouse model, which led to regression of these tumors upon systemic treatment with the prodrug 5-fluorocytosine; a prodrug which is converted to cytotoxic 5-fluorouracil (5-FU)—an anticancer agent (43). Recent studies further demonstrated that delivery of mRNA encoding prodrug-converting enzymes, yeast CD-UPRT (44) or HChrR6 (45), to cancer cells via EVs derived from tumor-tropic mesenchymal stem cells or HER2-directed EVs also resulted in tumor cell death. In this study, we showed that microvesicle-mediated delivery of MC-TK-NTR led to sustained transgene expression in the target breast cancer cells and efficiently produced direct and indirect cell killing in the tumor microenvironment after the treatment with prodrugs. We further demonstrated the number of tumor cells required to express TK-NTR for effective tumor regression. Our study demonstrated that *in vivo* delivery of MC encoding TK-NTR via microvesicles is a promising GDEPT approach and revealed quantified bystander effects. Previous studies of EV-mediated delivery of mRNA and/or protein for cancer therapy provided impetus for these further studies. We demonstrated that our approach provides an excellent platform for the delivery of tumor specific genes via specifically targeted EVs (46, 47, 48), and of tumor-activatable MCs that harbor tumor-specific promoters driving therapeutic genes such as TK-NTR (49).

Disclosure of Potential Conflicts of Interest

S.S Gambhir is a co-founder and holds equity in Earli Inc. which works in the field of early cancer detection; J.A. Ronald is a consultant for Earli Inc. No potential conflicts of interest were disclosed by the other authors.

Authors' Contributions

Conception and design: M. Kanada, B.D. Kim, J.W. Hardy, R. Paulmurugan, C.H. Contag

Development of methodology: M. Kanada, B.D. Kim, J.W. Hardy, M.P. Bernard, A.A. Zarea, S.A. Ibrahim, S.S. Gambhir, R. Paulmurugan

Acquisition of data (provided animals, acquired and managed patients, provided facilities, etc.): M. Kanada, B.D. Kim, J.W. Hardy, M.P. Bernard, G.I. Perez, T.J. Ge, A. Withrow, S.A. Ibrahim, V. Toomajian, R. Paulmurugan

Analysis and interpretation of data (e.g., statistical analysis, biostatistics, computational analysis): M. Kanada, B.D. Kim, J.W. Hardy, M.H. Bachmann, M.P. Bernard, A.A. Zarea, V. Toomajian, R. Paulmurugan, C.H. Contag

Writing, review, and/or revision of the manuscript: M. Kanada, J.W. Hardy, M.H. Bachmann, M.P. Bernard, A.A. Zarea, S.A. Ibrahim, S.S. Gambhir, R. Paulmurugan, C.H. Contag

Administrative, technical, or material support (i.e., reporting or organizing data, constructing databases): M. Kanada, R. Paulmurugan, C.H. Contag

Study supervision: M. Kanada, S.S. Gambhir, R. Paulmurugan, C.H. Contag

Other (reporter gene construct for extracellular vesicle detection): M.H. Bachmann

Acknowledgments

We thank Drs. A. Delcayre, A.C. Matin, J.H. Wang, M. Harada, and O. Vermesh for helpful discussions; Dr. A. Gilad for generously letting us use the C1000 Touch Thermal Cycler and ChemiDoc MP Imaging System; Drs. B. Hall and R. Thacker for supporting our imaging flow cytometry analysis; Dr. R. Eby for supporting our nanoparticle tracking analysis; Mr. J. Hix at the MSU IQ Imaging Core Facility; Ms. A. Porter at the MSU Investigative HistoPathology Laboratory; and Ms. E. Cox for her assistance in editing the article. This work was funded in part through a generous gift from the Chambers Family Foundation for Excellence in Pediatrics Research (to C.H. Contag), Grant 1UH2TR000902-01 from the NIH (to C.H. Contag), and the Child Health Research Institute at Stanford University (to C.H. Contag), and Start-up fund from Michigan State University (to M. Kanada).

The costs of publication of this article were defrayed in part by the payment of page charges. This article must therefore be hereby marked *advertisement* in accordance with 18 U.S.C. Section 1734 solely to indicate this fact.

Received March 20, 2019; revised June 13, 2019; accepted August 14, 2019; published first August 26, 2019.

References

1. Patel P, Young JG, Mautner V, Ashdown D, Bonney S, Pineda RG, et al. A phase I/II clinical trial in localized prostate cancer of an adenovirus expressing nitroreductase with CB1954 [correction of CB1984]. Mol Ther 2009;17:1292–9.
2. Morris JC, Ramsey WJ, Wildner O, Muslow HA, Aguilar-Cordova E, Blaese RM. A phase I study of intralesional administration of an adenovirus vector expressing the HSV-1 thymidine kinase gene (AdV.RSV-TK) in combination with escalating doses of ganciclovir in patients with cutaneous metastatic malignant melanoma. Hum Gene Ther 2000;11:487–503.
3. Searle PF, Chen MJ, Hu L, Race PR, Lovering AL, Grove JI, et al. Nitroreductase: a prodrug-activating enzyme for cancer gene therapy. Clin Exp Pharmacol Physiol 2004;31:811–6.
4. Karjoo Z, Chen X, Hatefi A. Progress and problems with the use of suicide genes for targeted cancer therapy. Adv Drug Deliv Rev 2016;99:113–128.
5. Lorenzer C, Dirin M, Winkler AM, Baumann V, Winkler J. Going beyond the liver: progress and challenges of targeted delivery of siRNA therapeutics. J Control Release 2015;203:1–15.
6. Knudsen KB, Northeved H, Kumar PE, Permin A, Gjetting T, Andresen TL, et al. *In vivo* toxicity of cationic micelles and liposomes. Nanomedicine 2015;11:467–77.
7. van der Meel R, Fens MH, Vader P, van Solinge WW, Eniola-Adefeso O, Schiffelers RM. Extracellular vesicles as drug delivery systems: lessons from the liposome field. J Control Release 2014;195:72–85.
8. Padma VV.An overview of targeted cancer therapy. Biomedicine 2015;5:19.
9. Raposo G, Stoorvogel W. Extracellular vesicles: exosomes, microvesicles, and friends. J Cell Biol 2013;200:373–83.
10. Kanada M, Bachmann MH, Contag CH. Signaling by extracellular vesicles advances cancer hallmarks. Trends Cancer 2016;2:84–94.
11. EL Andaloussi S, Mäger I, Breakefield XO, Wood MJ. Extracellular vesicles: biology and emerging therapeutic opportunities. Nat Rev Drug Discov 2013;12:347–57.
12. Kamerkar S, LeBleu VS, Sugimoto H, Yang S, Ruivo CF, Melo SA, et al. Exosomes facilitate therapeutic targeting of oncogenic KRAS in pancreatic cancer. Nature 2017;546:498–503.

13. Heusermann W, Hean J, Trojer D, Steib E, von Bueren S, Graff-Meyer A, et al. Exosomes surf on filopodia to enter cells at endocytic hot spots, traffic within endosomes, and are targeted to the ER. J Cell Biol 2016;213: 173–84.
14. Kanada M, Bachmann MH, Hardy JW, Frimannson DO, Bronsart L, Wang A, et al. Differential fates of biomolecules delivered to target cells via extracellular vesicles. Proc Natl Acad Sci U S A 2015;112: E1433–42.
15. McNeish IA, Tenev T, Bell S, Marani M, Vassaux G, Lemoine N. Herpes simplex virus thymidine kinase/ganciclovir-induced cell death is enhanced by co-expression of caspase-3 in ovarian carcinoma cells. Cancer Gene Ther 2001;8:308–19.
16. Jones RK, Pope IM, Kinsella AR, Watson AJM, Christmas SE. Combined suicide and granulocyte-macrophage colony-stimulating factor gene therapy induces complete tumor regression and generates antitumor immunity. Cancer Gene Ther 2000;7:1519–28.
17. Young JG, Green NK, Mautner V, Searle PF, Young LS, James ND. Combining gene and immunotherapy for prostate cancer. Prostate Cancer Prostatic Dis 2008;11:187–93.
18. Freytag SO, Rogulski KR, Paielli DL, Gilbert JD, Kim JH. A novel three-pronged approach to kill cancer cells selectively: concomitant viral, double suicide gene, and radiotherapy. Hum Gene Ther 1998;9: 1323–33.
19. Rogulski KR, Kim JH, Kim SH, Freytag SO. Glioma cells transduced with an Escherichia coli CD/HSV-1 TK fusion gene exhibit enhanced metabolic suicide and radiosensitivity. Hum Gene Ther 1997;8:73–85.
20. Bhaumik S, Sekar TV, Depuy J, Klimash J, Paulmurugan R. Noninvasive optical imaging of nitroreductase gene-directed enzyme prodrug therapy system in living animals. Gene Ther 2012;19:295–302.
21. Sekar TV, Foygel K, Willmann JK, Paulmurugan R. Dual-therapeutic reporter genes fusion for enhanced cancer gene therapy and imaging. Gene Ther 2013;20:529–37.
22. Sekar TV, Foygel K, Ilovich O, Paulmurugan R. Noninvasive theranostic imaging of HSV1-sr39TK-NTR/GCV-CB1954 dual-prodrug therapy in metastatic lung lesions of MDA-MB-231 triple negative breast cancer in mice. Theranostics 2014;4:460–74.
23. Darquet AM, Cameron B, Wils P, Scherman D, Crouzet J. A new DNA vehicle for nonviral gene delivery: supercoiled minicircle. Gene Ther 1997; 4:1341–9.
24. Kay MA, He CY, Chen ZY.A robust system for production of minicircle DNA vectors. Nat Biotechnol 2010;28:1287–9.
25. Riu E, Chen ZY, Xu H, He CY, Kay MA. Histone modifications are associated with the persistence or silencing of vector-mediated transgene expression *in vivo*. Mol Ther 2007;15:1348–55.
26. Tan Y, Li S, Pitt BR, Huang L. The inhibitory role of CpG immunostimulatory motifs in cationic lipid vector-mediated transgene expression *in vivo*. Hum Gene Ther 1999;10:2153–61.
27. Hyde SC, Pringle IA, Abdullah S, Lawton AE, Davies LA, Varathalingam A, et al. CpG-free plasmids confer reduced inflammation and sustained pulmonary gene expression. Nat Biotechnol 2008;26:549–51.
28. Huang M, Chen Z, Hu S, Jia F, Li Z, Hoyt G, et al. Novel minicircle vector for gene therapy in murine myocardial infarction. Circulation 2009;120: S230–7.
29. McCabe JB, Berthiaume LG.Functional roles for fatty acylated amino-terminal domains in subcellular localization. Mol Biol Cell 1999;10: 3771–86.
30. Lai CP, Kim EY, Badr CE, Weissleder R, Mempel TR, Tannous BA, et al. Visualization and tracking of tumour extracellular vesicle delivery and RNA translation using multiplexed reporters. Nat Commun 2015;6: 7029.
31. Shelke GV, Lässer C, Gho YS, Lötvall. Importance of exosome depletion protocols to eliminate functional and RNA-containing extracellular vesicles from fetal bovine serum. J Extracell Vesicles 2014;3:24783.
32. Liu F, Vermesh O, Mani V, Ge TJ, Madsen SJ, Sabour A, et al. The exosome total isolation chip. ACS Nano 2017;11:10712–23.
33. Jung MK, Mun JY.Sample preparation and imaging of exosomes by transmission electron microscopy. J Vis Exp 2018;131:e56482.
34. Multhaup M, Karlen AD, Swanson DL, Wilber A, Somia NV, Cowan MJ, et al. Cytotoxicity associated with artemis overexpression after lentiviral vector-mediated gene transfer. Hum Gene Ther 2010;21:865–75.
35. Mates L, Chuah MK, Belay E, Jerchow B, Manoj N, Acosta-Sanchez A, et al. Molecular evolution of a novel hyperactive Sleeping Beauty transposase enables robust stable gene transfer in vertebrates. Nat Genet 2009;41: 753–61.
36. Zhang Y, Zhang GL, Sun X, Cao KX, Ma C, Nan N, et al. Establishment of a murine breast tumor model by subcutaneous or orthotopic implantation. Oncol Lett 2018;15:6233–40.
37. Thakur BK, Zhang H, Becker A, Matei I, Huang Y, Costa-Silva B, et al. Double-stranded DNA in exosomes: a novel biomarker in cancer detection. Cell Res 2014;24:766–9.
38. McCormack E, Silden E, West RM, Pavlin T, Micklem DR, Lorens JB, et al. Nitroreductase, a near-infrared reporter platform for *in vivo* time-domain optical imaging of metastatic cancer. Cancer Res 2013;73:1276–86.
39. Fadok VA, Voelker DR, Campbell PA, Cohen JJ, Bratton DL, Henson PM. Exposure of phosphatidylserine on the surface of apoptotic lymphocytes triggers specific recognition and removal by macrophages. J Immunol 1992;148:2207–16.
40. Koopman G, Reutelingsperger CP, Kuijten GA, Keehnen RM, Pals ST, van Oers MH. Annexin V for flow cytometric detection of phosphatidylserine expression on B cells undergoing apoptosis. Blood 1994;84: 1415–20.
41. Hackett PB, Ekker SC, Largaespada DA, McIvor RS. Sleeping beauty transposon-mediated gene therapy for prolonged expression. Adv Genet 2005;54:189–232.
42. Yang L, Chiang Y, Lenz HJ, Danenberg KD, Spears CP, Gordon EM, et al. Intercellular communication mediates the bystander effect during herpes simplex thymidine kinase/ganciclovir-based gene therapy of human gastrointestinal tumor cells. Hum Gene Ther 1998;9:719–28.
43. Mizrak A, Bolukbasi MF, Ozdener GB, Brenner GJ, Madlener S, Erkan EP, et al. Genetically engineered microvesicles carrying suicide mRNA/protein inhibit schwannoma tumor growth. Mol Ther 2013;21:101–8.
44. Altanerova U, Jakubechova J, Benejova K, Priscakova P, Pesta M, Pitule P, et al. Prodrug suicide gene therapy for cancer targeted intracellular by mesenchymal stem cell exosomes. Int J Cancer 2018;144:897–908.
45. Wang JH, Forterre AV, Zhao J, Frimannsson DO, Delcayre A, Antes TJ, et al. Anti-HER2 scFv-directed extracellular vesicle-mediated mRNA-based gene delivery inhibits growth of HER2-positive human breast tumor xenografts by prodrug activation. Mol Cancer Ther 2018;17:1133–42.
46. Alvarez-Erviti L, Seow Y, Yin H, Betts C, Lakhal S, Wood MJ. Delivery of siRNA to the mouse brain by systemic injection of targeted exosomes. Nat Biotechnol 2011;29:341–5.
47. Ohno S, Takanashi M, Sudo K, Ueda S, Ishikawa A, Matsuyama N, et al. Systemically injected exosomes targeted to EGFR deliver antitumor microRNA to breast cancer cells. Mol Ther 2013;21:185–91.
48. Tian Y, Li S, Song J, Ji T, Zhu M, Anderson GJ, et al. A doxorubicin delivery platform using engineered natural membrane vesicle exosomes for targeted tumor therapy. Biomaterials 2014;35:2383–90.
49. Ronald JA, Chuang HY, Dragulescu-Andrasi A, Hori SS, Gambhir SS. Detecting cancers through tumor-activatable minicircles that lead to a detectable blood biomarker. Proc Natl Acad Sci U S A 2015;112:3068–73.